Optics Communications 381 (2016) 271–276

Contents lists available at ScienceDirect

Optics Communications

journal homepage: www.elsevier.com/locate/optcom

Ultrasonic photoacoustic spectroscopy of trace hazardous chemicals using quantum cascade laser

Deepak Kumar [a,*], Devinder Pal Ghai [a], R.K. Soni [b]

[a] Laser Science and Technology Centre, DRDO, Delhi 110054, India
[b] Department of Physics, Indian Institute of Technology Delhi, Hauz Khas, New Delhi 110016, India

ARTICLE INFO

Article history:
Received 16 February 2016
Received in revised form
15 June 2016
Accepted 6 July 2016
Available online 21 July 2016

Keywords:
Photoacoustic
Chemicals
Quantum Cascade laser
Laser Spectroscopy

ABSTRACT

We report an ultrasonic sensor based on open-cell photoacoustic spectroscopy method for the detection of explosive agents in traces. Experimentally, we recorded photoacoustic spectra of traces of hazardous explosives and molecules. Tunable mid-infrared quantum cascade lasers in the wavelength range 7.0–8.8 μm lying in the molecular fingerprint region are used as optical source. Samples of Pentaerylthirol Tetranitrate (PETN), Tetranitro-triazacyclohexane (RDX), Dinitrotoluene, p-Nitrobenzoic acid and other chemicals like Ibuprofen having quantity ~1.0 mg were detected using a custom made photoacoustic cells in both open and closed configurations. The explosive traces were swiped using paper from contaminated surface and detected. Finite element mesh based simulation of photoacoustic cell is carried out for optimization of geometry at ultrasonic frequency (40 kHz). A point sensor based on above approach will be very effective for forensic applications and suspicious material screening.

1. Introduction

Photoacoustic effect was invented by Alexander Graham Bell in 1880 while doing experiments on the transmission of sound via a beam of collimated sunlight [1]. The effect is basically an indirect effect of light, relying on thermally generated acoustic waves in a sample due to periodic irradiation of light. Photoacoustic Spectroscopy (PAS) is essentially a spectral study of photoacoustic effect on a sample. A thermal/acoustic signal generated due to light absorbed at different wavelengths give qualitative and quantitative information about a sample. The temperature rise in any sample is primarily governed by its non-radiative relaxation transitions. PAS is a highly sensitive method that can be used to detect trace levels of samples. It is an excellent spectroscopic tool for the study of materials in all three phases (solid, liquid and gas). PAS technique offers several advantages such as wide dynamic range, non-destructive detection, simplicity and compactness of experimental hardware. PAS has been widely used in diverse fields such as atmospheric sciences, combustion process, medical diagnosis, homeland security, food industry and atmospheric pollution monitoring. The invention of quantum cascade lasers (QCL) has boosted the research in the field of Photoacoustic Spectroscopy. Availability of room temperature operation of QCL and broad tunability in the molecular vibrational fingerprinting band, typically 500–1500 cm^{-1} has enhanced selectivity and opened new avenues for PAS based sensors [2–4]. Applicability of photoacoustic spectroscopy to various spectroscopic measurements is discussed by Gary A. West et al., applications like linear absorption spectroscopy (vibrational and electronic), vibrational overtone spectroscopy, trace analysis, reaction kinetics and nonlinear spectroscopy (multiphoton as well stimulated Raman scattering) and photoacoustic Raman spectroscopy (PARS) and myriad applications to gaseous trace component analysis has been reviewed and discussed [5]. In year 2008, pulsed external-cavity quantum-cascade laser (EC-QCL) tunable in 9.3–0.10 μm band was used for the acquisition of mid-IR photoacoustic (PA) spectra of solids [6]. Researchers have demonstrated detection of solid traces of RDX, PETN, TNT, and TBP adsorbed on surfaces with a limit of detection of 100 ng/cm^2 and a standoff distance of 20 m using a reverse photoacoustic spectroscopy employing EC-QCL [7]. Pietro Patimisco, et al. has reviewed the Quartz-Enhanced Photoacoustic Spectroscopy (QEPAS) for gaseous species concentration monitoring. Quartz enhanced photoacoustic spectroscopy employs a resonant quartz crystal tuning fork as the detector. The technique has shown best gaseous species detection sensitivity in the mid-IR fingerprint range where powerful QCLs are available, sensitivity of QEPAS has reached record detectable trace gas concentration levels in part-per-trillion range [8].

Xing Chen et al. reported standoff detections of TNT powder from a range of 240 cm of quantity 1 mg, using 7.35 μm quantum cascade lasers (QCLs) based photoacoustic (PA) experiments [9].

* Corresponding author.
E-mail addresses: deepakkumar@lastec.drdo.in (D. Kumar), ravisoni@physics.iitd.ac.in (R.K. Soni).

http://dx.doi.org/10.1016/j.optcom.2016.07.017
0030-4018/

Photothermal cantilever deflection spectroscopy (PCDS) based quantification of picogram levels of ternary mixtures of similar explosives (trinitrotoluene (TNT), cyclotrimethylene trinitramine (RDX), and pentaerythritol tetranitrate (PETN)) using nano-mechanical IR spectroscopy has been reported [10]. Highly resolved IR bands of RDX and TNT sample and their soil mixtures were recorded in the 9.6 and 10.6 mm regions of the CO_2 laser [11]. Acoustically open ultrasonic photoacoustic detector having optically multipass arrangement has been reported for trace gas and atmospheric pollution studies using CO_2 laser source [12]. Photoacoustic (PA) signals were detected by Gianfranco Giubileo and Adriana Puiuin in the entire frequency 9–11 μm band of CO_2 laser by their home-made photoacoustic apparatus. The Laser PAS spectral absorptions recorded with a CO_2 laser source were reported for 2, 4-DNT; 2, 6-DNT; HMX; TATP; PETN; TNT and RDX having concentrations ~100 μg [13]. PAS measurements of solid explosive material /energetic material covering the wavelength region of 400–1600 nm were reported using xenon and halogen lamps as a source [14].

The aim of the present work is to carry out the mid-infrared photoacoustic spectroscopy of microgram level quantity of energetic materials and other chemicals in ultrasonic regime (40 kHz) using open acoustic resonator cell geometry. The aim is also to develop an Open-Cell Laser Photoacoustic Spectroscopy (OC-LPAS) Sensor for rapid detection of suspicious traces.

2. Theory

The primary source of acoustic signal in a photoacoustic cell arises from the periodic heat flow from the solid to the surrounding gas as the solid is cyclically heated by the chopped/modulated light. Only a relatively thin layer of air adjacent to the surface of the solid responds thermally to the periodic heat flow from the solid to the surrounding air via piston effect. This boundary layer of air can then be regarded as a vibratory piston, resulting in generation of acoustic signals in the cell. Since the magnitude of the periodic pressure fluctuations in the cell is proportional to the amount of heat emanating from the solid absorber, there is a close connection between the strength of the acoustic signal and the amount of light absorbed by the solid [15,16]. Theory of photoacoustic effect in solids was formulated by Rosencwaig and Gersho. With regard to solid samples there are three important parameters which are as listed below: 1. Sample thickness 'l', 2. Optical absorption length '$\mu_\beta = 1/\beta$', where β is the optical absorption coefficient in cm^{-1} and 3. Thermal diffusion length 'μ_t', which determine how far a periodic wave can travel into a solid without dissipation.

$\mu_t = \sqrt{\frac{2.\alpha}{\omega}}$, where '$\alpha$' is thermal diffusivity of medium ($\alpha = \frac{k}{\rho.C}$); k is thermal conductivity, ρ is the density of medium and C is the specific heat capacity of medium and 'ω' is the frequency of heat waves (radians/s) or the chopping frequency of laser. It is clear that the thermal diffusion length is inversely proportional to the chopping frequency and hence at higher frequency in ultrasonic band the thermal diffusion length is very small as compare to audio frequencies. Under the condition of thermal diffusion length 'μ_t' being smaller than optical absorption length 'μ_β', photoacoustic spectrum will be a true representation of the optical absorption spectrum, otherwise the property of backing material would also come into the measurement. In Photoacoustic measurements of solid samples, the acoustic response of the air above the sample is measured and related to the thermal properties of the sample. The time dependent component of the temperature of solid in the surrounding gas/air attenuates rapidly with increasing distance from the surface of the solid. The boundary of air, which

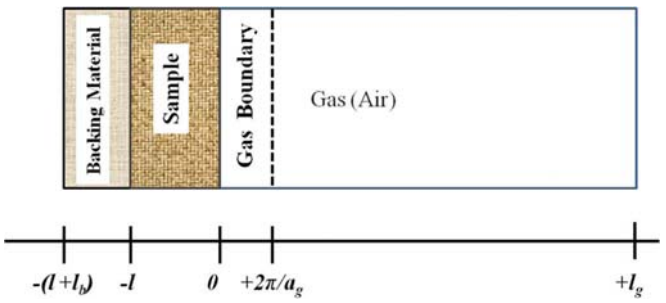

Fig. 1. Cross-sectional view of a simple photoacoustic cell.

respond thermally to the periodic temperature at solid gas interface is $2.\pi/a_{gas}$, where a_{gas} is known as the thermal diffusion coefficient of surrounding gas. The typical value of air boundary is $2.\pi/a_{gas}$ ~0.2 cm for a chopping rate of 100 Hz. In the study presented in this paper the air boundary length decreases to 0.008 cm at chopping frequency 40,000 Hz.

2.1. Simulation and theoretical analysis

Fig. 1 shows a typical cross section of photoacoustic cell, showing the positions of a solid sample, backing material and gas column. According the Rosencwaig and Gersho (RG) one dimensional thermal diffusion model the photo-acoustic signal intensity δp (physical pressure variation due to modulated light source) is given as

$$\delta p = \frac{(1-j)\beta.\, l.\, \mu_b.\, Y}{2.\, a_g.\, k_b} \tag{1}$$

where a_g, μ_b, k_b, l and β are the thermal diffusion coefficient of air (cm^{-1}); the thermal diffusion length of the backing material (cm), the thermal conductivity of the backing material (W/m K), the film thickness and the optical absorption coefficient of the film (cm^{-1}) for the wavelength λ, respectively; and Y as a constant factor. The acoustic signal is thus proportional to $\beta.l$ which means that the whole sample length contributes to photoacoustic signal. For the thermally thin case in which thermal diffusion length $\mu_t \gg l$, the thermal properties of the backing material come into play in the expression for photoacoustic signal intensity (Pascal). The factor 'Y' appearing in the above equation is $Y = \frac{\gamma.P_0.I_0}{2\sqrt{2}.l_g.T_0}$, where γ is the ratio of specific heats at constant pressure and volume, I_0 is the incident, monochromatic light flux (W/cm^2), P_0 and T_0 are is ambient pressure and temperature respectively and l_g is length of gas column above the sample.

Fig. 2 shows a variation of the thermal diffusion length of RDX powder with chopping frequency and its comparison with the optical penetration length. As an estimation, a 10 μg weight of RXD with a uniform thickness having a diameter of 4 mm on paper

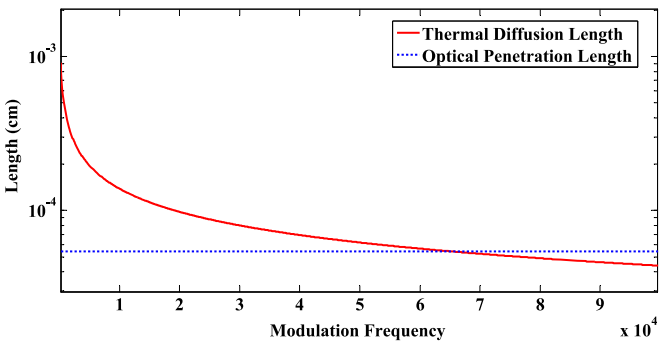

Fig. 2. Comparison of optical and thermal diffusion length for RDX powder.

Please cite this article as: D. Kumar, et al., Optics Communications (2016), http://dx.doi.org/10.1016/j.optcom.2016.07.017

swipe corresponds to a sample physical thickness of $l=0.44\,\mu m$. The RDX has an extinction coefficient 1.153 @ 1268.7 cm^{-1} resulting in an optical penetration depth $\mu_\beta=0.54\,\mu m$ @ 1268.7 cm^{-1} [17]. RDX has a thermal conductivity $k=2.53\times10^{-4}$ cal/cm S °C, density $\rho=1.804$ g/cm^3 and specific heat capacity C=0.232 cal/g °C which results in thermal diffusivity $\alpha=k/\rho.C=6.0\times10^{-4}$ cm^2/s and the thermal diffusion lengths $\mu_t=\sqrt{\frac{2.\alpha}{\omega}}$, [18]. Plot in Fig. 2 shows that for 1268.7 cm^{-1} excitation and for modulation frequencies below 65 kHz the RDX sample is thermally thin and above 65 kHz the sample is thermally thick. For modulation frequencies below 65 kHz the thermal properties of backing material must be taken into consideration for RDX.

3. Photoacoustic cell design

In the design of photoacoustic cell, we have considered the design principle of PAS resonators of different shapes such as pipes, cylinders, and spheres [19,20]. The indigenous T-shaped photoacoustic cell is fabricated using stainless steel material. The cell consists of two hollow cylinders intersecting each other in a perpendicular geometry. The vertical cylinder has a height of 2.36 cm and diameter 2.0 cm and horizontal cylinder has a height of 3.0 cm and a diameter of 0.7 cm. The dimensions of cell are optimized for 40 kHz resonant frequency. Both the open and closed geometries of cell were used for conducting the experiments and simulations. The acoustic resonant Eigen-frequencies of a simple open or closed cylinder can be calculated analytically. Since direct analytical solutions of Eigen-frequencies of T-cell are not available so the COMSOL pressure acoustic simulations based on Finite-element mesh (FEM) are carried out for both open and closed geometries to optimize the resonant frequency of T-cell at ultrasonic frequency centered at 40 kHz. The Eigen frequency and Eigen-modes are obtained by solving the following differential equation.

$$\vec{\nabla}^2\left(\frac{p(\vec{r})}{\rho}\right)+\left(\frac{\omega}{c}\right)^2\frac{p(\vec{r})}{\rho}=0 \tag{2}$$

where $p(\vec{r})$ is the pressure generated by the photoacoustic effect. Acoustic pressure given by $p=p_0.e^{i.\omega.t}(N/m^2)$ is a harmonic quantity for the pressure acoustics frequency domain study, as described in Eq. (1) as photo-acoustic signal intensity δp. 'ω' is the angular frequency, 'ρ' is the density of air (1.2 kg/m^3) and 'c' is the speed of sound in air (343) m/s at STP. The walls of photoacoustic cell are sound hard boundaries leading to the normal derivative of pressure to vanish at boundaries i.e.

$$\hat{n}.\left(\frac{1}{\rho}.\nabla p\right)=0 \quad .... \tag{3}$$

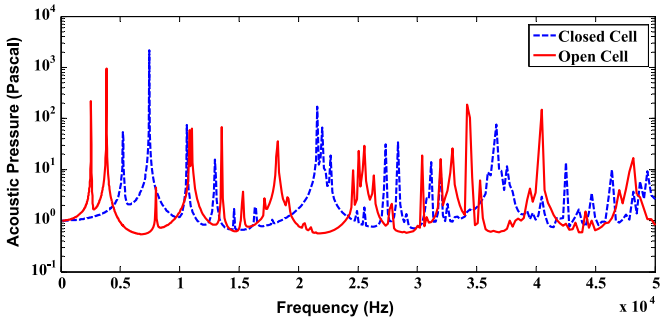

Fig. 3. Variation of Acoustic Pressure vs. Frequency for Open and Closed Cell Geometry.

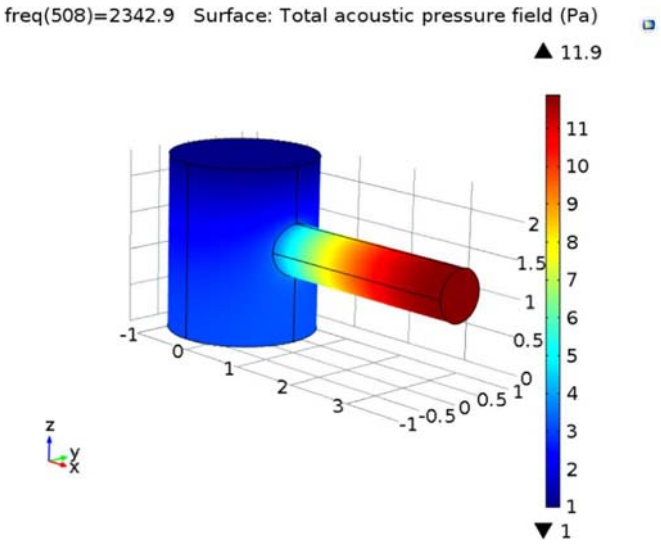

Fig. 4. Simulated Acoustic pressure field for the first resonant frequency of open cell. (For interpretation of the references to color in this figure legend, the reader is referred to the web version of this article.)

where 'n' is the outward pointing unit normal vector seen from inside the geometry of T-cell. The pressure inside the cell is taken as 1 Pa and all the boundaries are taken as sound hard boundaries except the top surface of vertical cylinder in case of open cylinder. In case of closed cylinder, all the boundaries are taken as sound hard. Five quadratic elements should be used to resolve each wavelength. Therefore, the maximum mesh element size is set to 1/5 of the shortest wavelengths present, i.e. mesh size is taken $c/5.f_{max}$, f_{max} is the maximum frequency for which solutions are to be evaluated. Finite Element Mesh (FEM) simulations of PAS Cell provide the results of pressure acoustics frequency domain study. Fig. 3 shows the response of PAS cell, i.e. average acoustic pressure integrated over the volume with frequency up to 50 kHz for open and closed geometry. A total of 1000 frequencies in the 1–50 kHz band are solved. The design of the cell is optimized in the present case to get a pressure acoustic maximum at 40 kHz frequency for open cell geometry. It is also apparent from Fig. 3 that at 40 kHz, the average integrated acoustic pressure for open-cell configuration is more than the close-cell configuration.

Fig. 4 shows simulated cell geometry and the acoustic pressure field variation for first resonant frequency, i.e. 2342.9 Hz showing the maximum pressure field in red color (dark color in print version) in the horizontal cylinder. The vertical color scale shows the acoustic pressure variations for the PAS cell. It is understandable from the Fig. 4 that the first resonant mode is a longitudinal one. The resonant acoustic mode at 40 kHz too is a longitudinal mode having an acoustic resonant mode number 12.

4. Experimental set-up

A schematic diagram of the experimental setup is shown in (Fig. 5a). The commercially available QCL sources from M/s. Daylight Solutions, model number Uber Tuner UT-10 (tuning range 1130–1420 cm^{-1}) with increment wavelength of 1 cm^{-1} is used. The laser is having an accuracy of 1 cm^{-1} and a linewidth of ~0.5 cm^{-1}. The QCL laser beam is modulated by pulses of 500 ns duration at the frequency 40 kHz using a function generator, the maximum average power of the laser is 35 mW at peak of intensity profile @100 kHz modulation. Laser intensity does not damage the samples, as the average laser power is ~10 mW and in addition

Please cite this article as: D. Kumar, et al., Optics Communications (2016), http://dx.doi.org/10.1016/j.optcom.2016.07.017

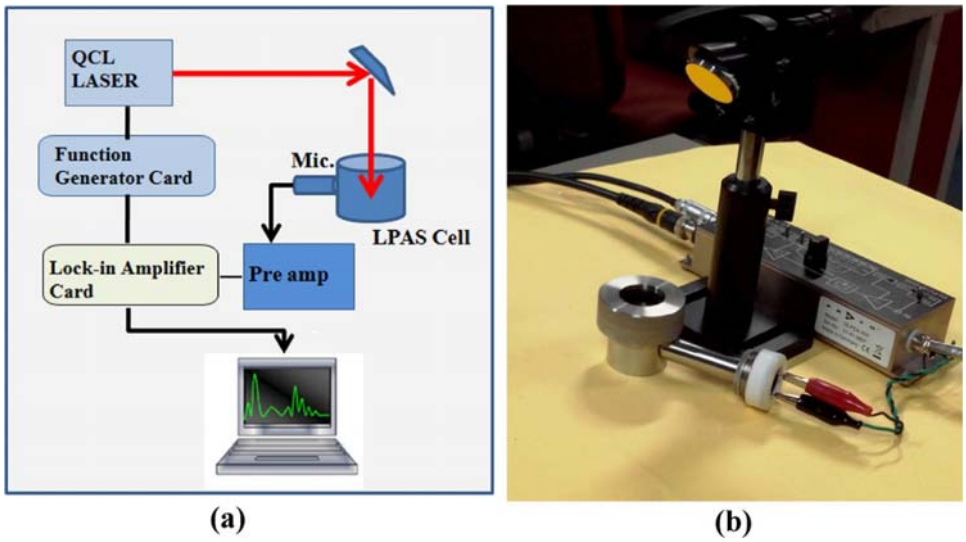

Fig. 5. (a) Experimental arrangement, (b) PAS Cell with amplifier.

the laser beam is not focused. Dual channel function generator (Tektronix AFG3102) is used to modulate the laser and to give the reference signal to lock-in-amplifier. The laser is incident on photoacoustic T-cell though the vertical cylinder as shown in (Fig. 5b). The vertical cylinder is kept open as well as closed for different measurements. A calcium fluoride window is used for the closed configuration to allow the laser beam to pass through it. The absorption of tunable laser radiation by the sample is followed by non-radiative decay resulting in pressure fluctuations at modulation frequency which were detected by a sensitive microphone attached at the one of end of horizontal cylinder. A commercially available microphone detector (Murata MA40B5R) is used as a PAS sensor. Sensitivity of the detector is -63 dB with a sound pressure level 0 dB$=$20 μPa. For the pre-amplification of PAS signal, 500 kHz bandwidth current amplifier (Femto de, DLPCA-200) having input noise 43 femto ampere/$\sqrt{\text{Hz}}$ is used at bandwidth 50 kHz settings. Amplified PA signal from the current amplifier is fed to a lock-in-amplifier (SR830 DSP Stanford Research). The time constant of measurement of Lock-in-amplifier is taken as 100 ms and sensitivity in 100 μV to 10 mV scales. The analog signal from lock-in amplifier are digitized using a multifunction data acquisition card (USB 4716 Advantech) and recorded on a computer having a Labview based graphical user interface. All the spectra were recorded by fast forward scanning mode of Quantum Cascade Laser (QCL) which limits the wavelength accuracy of ± 2 cm^{-1}. Initial experiments were carried out using carbon black as a reference sample. Powders as well as traces of molecules swiped using paper soaked with alcohol were studied. The swiping paper folded into L-shape was placed directly into the vertical cylinder of the T-shape PAS cell. Traces were swiped using the upper face of the horizontal L-shape of paper. Before placing in the cell it was ensured that the alcohol has got evaporated from the paper. All the experiments are carried out at room temperature of 26 °C in laboratory conditions and relative humidity around 40%.

5. Results and discussion

The Laser photoacoustic spectroscopy (LPAS) spectra of the samples of 2, 4 dinitrotoluene (DNT), Tetranitro-triazacyclohexane (RDX), Pentaerylthirol Tetranitrate (PETN),

p-Nitrobenzoic acid (PNBA) and isobutylphenylpropanoic acid (Ibuprofen) were recorded as shown in Fig. 6. All the spectra presented here were recorded using open cell configuration

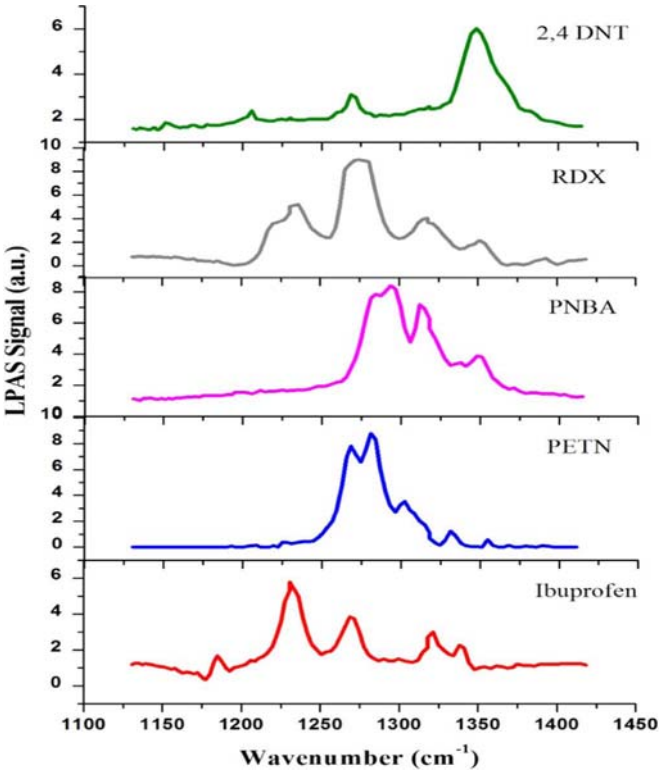

Fig. 6. LPAS spectra of various molecules.

without averaging the signal intensity, i.e. all the spectra are generated using a single forward wavelength scanning of laser. PAS spectra were observed to have a very good repeatibility in terms of spectral peak positions and relative PAS intensities. The present method aims at the detection of suspected visible contamination on any surface. The visually suspected contamination on any surface has a concentration in micrograms and can be swiped easily using paper soaked in a volatile liquid like alcohol. We were able to record spectra of samples having concentration of the order 1.0–10 mg. The concentration of swipe samples on paper was verified by depositing the alcohol solution of explosives on a quartz crystal microbalance. In case of the closed cell configuration PAS signal could only be recorded for higher concentrations ($\sim$mg) as the cell geometry is optimized for open cell configuration. Ultrasonic

Please cite this article as: D. Kumar, et al., Optics Communications (2016), http://dx.doi.org/10.1016/j.optcom.2016.07.017

Table 1
Comparison of experimental PAS peaks with literature with assignments.

PAS peaks (cm^{-1}), Present work	Infrared Peaks (cm^{-1}) [Ref.]	Vibrational mode	Strength
2, 4 Dinitrotoluene [22,23]			
1348	1346	2,4 NO_2 symmetric stretching	Strong broad
1266	1268	C–H (ring) bend	Strong
1205	1204	Ring breathing, C–H (ring) bend	Weak
RDX			
1392	1390 [25], 1395 [24]	C–N stretch	Strong
1354	1351 [25], 1358 [24]	C–N stretch	Strong
1316	1312 [25], 1310 [24]	N–N stretch	Strong broad
1272	1269 [25], 1270 [24]	C–N stretch	Very strong
1236	1234 [25], 1235 [24]	C–N stretch	Strong Overlap
1221	1220 [24]	C–N stretch	Strong overlap
PETN			
1305	1306 [25], 1306 [26,27]	CH_2 wag+C5 skeletal+NO_2 rock	Medium overlap
1283	1286 [25], 1285 [26,27]	NO_2 stretch+CH bend+C5 skeletal	Very strong overlap
1270	1272 [25], 1272 [26,27]	CH_2 bend+C5 skeletal+ONO_2 rock	Strong overlap
Ibuprofen [29]			
1324	1321	C –H bend+CO–H in-plane bending	Strong
1270	1269	C –H bend+CO–H in-plane bending	Strong
1232	1231	CO–H in-plane bending	Very Strong

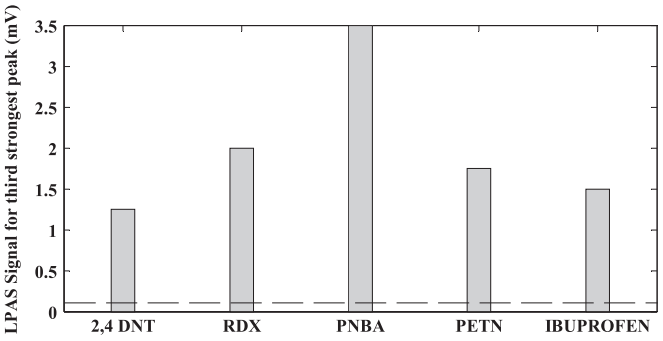

Fig. 7. Bar graph of LPAS signals (mV) at lock-in amplifier for 1 mg quantity of various molecules, noise level (100 micro volts) is shown as a dashed line.

(40 kHz) modulation frequency improved the PAS signal in two manners, firstly, the laser average power increase at higher modulation frequency and secondly at 40 kHz the ambient acoustic noise is low as compared to lower frequencies in the acoustic domain. Ultrasonic modulation frequencies also lower the thermal diffusion length in sample and therefore reduce the PAS background due to the backing material. Average noise amplitude in a laboratory environment corresponds to level 10^{-4}–10^{-2} Pa in the audio frequency band and reduces to $\sim 10^{-5}$–10^{-4} Pa at 40 kHz band [21], which facilitates a very good acoustic isolation of the PA cell for ultrasonic frequencies.

A Photoacoustic spectrum of paper is recorded in the spectral band 1130–1420 cm^{-1} and it was observed that the LPAS spectrum of paper does not have any distinct peak in this band. Rather a continuous broad response in entire band is observed. It must also be noted that, in all LPAS measurements a wavelength accuracy and repeatability of ± 2 cm^{-1} is observed,which is limited by the fast scanning mode of the QCL.

Table 1 elaborates the experimentally observed peaks for different molecules which are compared with those reported in literature. It can be seen that the experimentally obtained peaks are in very close agreement with the reported literature. For 2, 4 DNT, which is basically a precursor of Trinitrotoluene (TNT), a very strong peak is observed at 1348 cm^{-1} manifested due to –NO_2 symmetric stretching, Fourier Transform Infrared (FTIR) Spectra and peak assignments previously reported by reference [22,23] are taken as reference for 2, 4 DNT. In case of RDX, a very strong peak at 1272 cm^{-1} is observed due to C–N stretch vibrational mode. Strong overlapping peaks at 1221 and 1236 cm^{-1} are distinctively resolved in our experimental measurements. Spectral positions as well as relative Photoacoustic intensities are in agreement with FTIR spectra reported in the literature having resolution 4 cm^{-1} [24,25]. Strong overlapping peaks at 1270 cm^{-1} ($-NO_2$ Stretching) and 1283 cm^{-1} ($-CH_2$ bending) were distinctively resolved for PETN and are in agreement with reported values [26,27]. In addition to the NO_2 stretching motion, this mode contains significant contributions from a $-$CH bend and C_5 skeletal deformation. For PNBA, the photoacoustic spectrum is shown to have peaks at 1284 cm^{-1}, 1294 cm^{-1}, 1313 cm^{-1}, 1342 cm^{-1} and 1352 cm^{-1}. Peak at 1294 cm^{-1} (very strong) is due to C–OH stretching and peak at 1352 cm^{-1} (very strong) is due to symmetric –NO_2 stretching. The recorded spectra are in close agreement with literature reported FTIR spectra having wavenumber resolution of 1 cm^{-1} [28]. Ibuprofen is reported to have a very strong absorption at 1232 cm^{-1} due to CO–H in-plane bending agrees well with our measurements [29]. Peaks at 1270 and 1324 cm^{-1} are mixed modes having a C–H bend + CO–H in-plane bending. It was observed that with concentration less than 1 mg and keeping the sensitivity of lock-in-amplifier in microvolt scale, the ambient water vapor spectral signature becomes a source of noise for open cell configuration.

For the determination of limits of detection (LOD) we have considered the third strongest peak of the spectrum as the

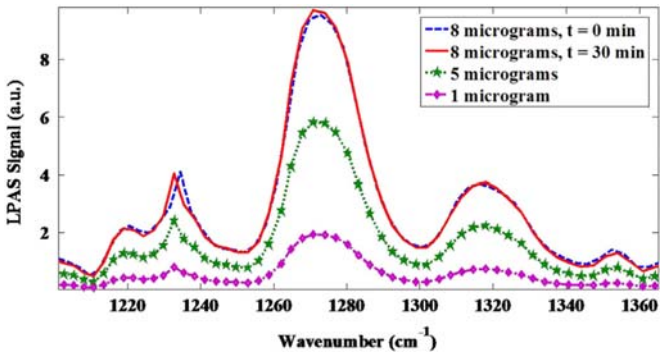

Fig. 8. LPAS signal of RDX of different quantity. (For interpretation of the references to color in this figure legend, the reader is referred to the web version of this article.)

Please cite this article as: D. Kumar, et al., Optics Communications (2016), http://dx.doi.org/10.1016/j.optcom.2016.07.017

reference peak. As at least three peaks in the tunability of our laser provides a fairly good chance of molecular identification. For example, in case of RDX molecule the strongest peak is at 1272 cm^{-1}, second strongest peak is at 1236 cm^{-1} and the third strong peak happens to be at 1316 cm^{-1}. The peaks at 1205 cm^{-1}, 1316 cm^{-1}, 1313 cm^{-1}, 1305 cm^{-1} and 1324 cm^{-1} are taken as reference for 2, 6 DNT, RDX, PNBA, PETN and Ibuprofen respectively. Fig. 7 is a bar-chart; each bar shows the photoacoustic signal corresponding to a concentration of 1 μg of all above said molecules. For our experimental set-up, we have taken a 100 μV signal as the noise level at the input of lock-in-amplifier. The dashed horizontal line represents the noise floor (100 μV) of our sensor. For a signal to noise ratio (SNR) of 10 the signal levels 1 mV is required. It can be seen in Fig. 7 that for the 1 mg quantity the SNR is typically over 10 for all of the molecules.

Fig. 8 shows the RDX spectra recorded using different quantities from 1 to 8 mg. To display the repeatibility and the time evolution of present sensor, two of spectra (solid red and dashed blue lines) are produced, both recorded in an interval of 30 min for the 8 mg quantity. The spectra show a very good repeatability in terms of peak position as well as relative spectral intensities. The spectrum corresponding to 5 mg quantity (dot green line with star marker) and 1 mg (dashed dot purple line with diamond marker) shows the LPAS signal variations. All the spectra show repeatability in terms of peak spectral positions. Also, it is discernible from the Fig. 8, that one microgram concentration is easily detectable.

6. Conclusions

We have reported an open-cell laser photoacoustic spectroscopy (OC-LPAS) sensor using tunable pulsed quantum cascade laser source. This system is capable of rapid detection of explosive traces on paper swipes having concentration ~1.0 mg. Powder, gel and liquid samples can also be studied with a slight modification. The sensor discriminates various molecules in the fingerprinting vibrational band with a very good repeatibility and signal to noise ratio >10. No averaging of spectra is required and the total measurement time is less than 10 s. The open-cell LPAS spectra peaks are in close agreement with the reported literature. The described method is non-invasive in nature, have an easy sample preparation method. Open cell offers easy access to the measurement compartment and do not require any transparent optical window. Employment of the ultrasonic detector ensures insensitivity to ambient acoustic noise. Ultrasonic modulation frequencies lower the thermal diffusion length, therefore, reduce the PAS background due to the backing material. A point sensor based on above approach offers wide potential for explosive trace detection, forensic applications, post blast residue analysis and suspicious material screening. A more sensitive microphone with a broad ultrasonic responsivity band can be used in future to improve the detection sensitivity of the sensor. Finite-element mesh based simulation of photoacoustic cell is used for optimization its geometry at ultrasonic frequency (40 kHz). The present method deals with pure molecules, we are striving to incorporate algorithm to identify molecules from a mixture.

Acknowledgments

Authors are thankful to Sh. Hari Babu Srivastava, Director LASTEC, for his encouragement and support for carrying out this work. Authors are thankful to Dr. Ramesh C Sharma for providing access to the experimental facilities. Thanks are due to Ms. Gaganpreet for helping in plotting the spectra.The authors also wish to thank Ms. Usha Kumari and Mr. Umesh Sah for their help during the experiments and Mr. Shiv Kishor for in-house fabrication of the photoacoustic cell.

References

[1] A.G. Bell, Am. J. Sci. 20 (1880) 305.
[2] J. Faist, F. Capasso, D.L. Sivco, C. Sirtori, A.L. Hutchinson, Science 264 (1994) 553–556.
[3] J.S. Li, W. Chen, H. Fischer, Appl. Spectrosc. Rev. 48 (2013) 523–559.
[4] R.F. Curl, F. Capasso, C. Gmachl, A.A. Kosterev, B. McManus, R. Lewicki, M. Pusharsky, G. Wysocki, F.K. Tittel, Chem. Phys. Lett. 487 (2010) 1–18.
[5] Gary A. West, Joseph J. Barrett, Donald R. Siebert, K. Virupaksha Reddy, Rev. Sci. Instrum. 54 (1983) 797.
[6] Qing Wen, Kirk H. Michaelian, Opt. Lett. 33 (16) (2008) 1875–1877.
[7] C.W. Van Neste, L.R. Senesac, T. Thundat, Anal. Chem. 81 (5) (2009) 1952–1956.
[8] Pietro Patimisco, Gaetano Scamarcio, Frank K. Tittel, Vincenzo Spagnolo, Sensors 14 (2014) 6165–6206.
[9] Xing Chen, Dingkai Guo, Fow-Sen Choa, Chen-Chia Wang, Sudhir Trivedi, A. Peter Snyder, Guoyun Ru, Jenyu Fan, Appl. Opt. 52 (12) (2013) 2626–2632.
[10] Seonghwan Kim, Dongkyu Leel, Xunchen Liu1, Charles Van Neste, Sangmin Jeon, Thomas Thundat, Nat. Sci. Rep. 3 (2013) 1111.
[11] R.L. Prasad, R. Prasad, G.C. Bhar, S.N. Thakur, Spectrochim. Actat A 58 (2002) 3093–3102.
[12] András Miklós, Shan-Chuang Pei, A.H. Kung, Appl. Opt. 45 (11) (2006) 2529–2534.
[13] Gianfranco Giubileo, Adriana Puiuin, Nucl. Instrum.s Methods Phys. Res. Sect. A 623 (2010) 771–777.
[14] Kazuo Hasue, Shoji Nakahara, Jun Morimoto, Tetsuo Yamagami, Yoichi Okamoto, Toru Miyakawa, Propellants Explos. Pyrotech. 20 (1995) 187–191.
[15] A. Rosencwaig, A. Gersho, Science 190 (1975) 556–557.
[16] A. Rosencwaig, A. Gersho, J. Appl. Phys. 47 (1976) 64–69.
[17] Clayton S.C. Yang, Barry R. Williams, Ashish Tripathi, Melissa S. Hulet, Alan C. Samuels, Joseph A. Domanico, Joseph May, Ronald W. Jr. Miles, Augustus W. III Fountai, ECBC-TR-1243, U.S. Army Edgewood Chemical Biological Centre, 2014.
[18] John F. Baytos, LA-8034-MS, Los Alamos Scientific Laboratory, 1979.
[19] Andra´s Miklo´s, Peter Hess, Rev. Sci. Instrum. 72 (4) (2001) 1937–1955.
[20] Method Bernd Baumann, Bernd Kost, Hinrich Groninga, Marcus Wolff, Rev. Sci. Instrum. 77 (2006), 044901-044901.
[21] Randall P. Reynolds, Will L. Kinard, Jesse J. Degraff, Ned Leverage, John N. Norton, J. Am. Assoc. Lab. Anim. Sci. 49 (5) (2010) 592–597.
[22] Carmen M. Ramos, Liliana F. Alzate, Neiza M. Herna'ndez, Samuel P. Herna ´ndez, Nairmen Mina, J. Mol. Struct.: Theochem. 769 (2006) 69–76.
[23] J.J.P. Stewart, S.R. Bosco, W.R. Carper, Spectrochim. Acta A: Mol. Spectrosc. 42 (1) (1986) 13–21.
[24] F. Pristera, M. Halik, A. Castelli, W. Fredericks, Anal. Chem. 32 (1960) 495.
[25] A. Banas, K. Banas, M. Bahou, H.O. Moser, L. Wen, P. Yang, Z.J. Li, M. Cholewa, S. K. Lim, Ch.H. Lim, Vib. Spectrosc. 51 (2009) 168–176.
[26] S.V. Ingale, P.B. Wagh, P.U. Sastry, A.K. Patra, R. Tewari, I.K. Singh, S.B. Phapale, R.D. Wasnik, A. Subhananda Rao, Satish C. Gupta, Def. Sci. J. 61 (6) (2011) 534–539.
[27] Yuri A. Gruzdkov, Yogendra M. Gupta, J. Phys. Chem. A 105 (2001) 6197–6202.
[28] M. Samsonowicz, R. S´Wisłocka, E. Regulska, W. Lewandowski, Int. J. Quantum Chem. 107 (2007) 480–494.
[29] M.L. Vueba, M.E. Pina, L.A.E. Batista De Carvalho, J. Pharm. Sci. 97 (2) (2008) 845–859.

Please cite this article as: D. Kumar, et al., Optics Communications (2016), http://dx.doi.org/10.1016/j.optcom.2016.07.017